RSC Advances

PAPER

Cite this: *RSC Adv.*, 2018, **8**, 37396

Broadband ultraviolet to near infrared conversion in Eu^{2+},Nd^{3+} co-doped $SrAl_2O_4$

Yuping Tai,[a] Bingli Pan,*[a] Xinzhong Li,[b] Zhaogang Nie,[c] Xigang Du[a] and Guanghui Yuan[d]

Received 23rd September 2018
Accepted 31st October 2018

DOI: 10.1039/c8ra07898j

rsc.li/rsc-advances

In this study, we investigated the quantum cutting (QC) mechanism in Eu^{2+}–Nd^{3}-co-doped $SrAl_2O_4$ microcrystals by fluorescence spectroscopy and decay lifetime analysis. In this material, the near-infrared (NIR) emissions of Nd^{3+} in the range of 800–1200 nm were enhanced under the excitation of the Eu^{2+}:$4f^7 \rightarrow 4f^65d^1$ transition radiation. The lifetime of the $5d^1$ level of Eu^{2+} decreased with the increase in the Nd^{3+} concentration. These results verified the occurrence of cooperative energy transfer (CET) from the Eu^{2+}:$5d^1$ excited state to the Nd^{3+}:$^4F_{3/2}$ level, by which one absorbed ultraviolet-visible photon was converted to two NIR photons with an optimal quantum efficiency (QE) of approximately 177.1%. Therefore, this broadband QC material paves the way for a further increase in the conversion efficiency of c-Si solar cells.

1. Introduction

With the rapid development of the global economy and industry the traditional energy resources face the problems of exhaustion and serious environmental pollution. Solar energy is a representative alternative clean energy with significant advantages: it is abundant, non-pollution, and inexhaustible. The solar energy supplied from the sun is approximately 10 000 times higher than the current energy consumption on the Earth.[1] Therefore, it becomes the most promising energy resource of interest to national governments. Since its development in the previous century, the silicon solar cell has been extensively employed in various industries owing to its low cost, optimized preparation technology, and high efficiency.[2–4] However, silicon has a band-gap of 1.12 eV and thus it can only absorb near-infrared (NIR) photons in the solar spectrum range of 900–1200 nm; the majority of the energy in the ultraviolet-visible (UV-Vis) region is lost owing to thermalization of charge carriers, referred to as spectral mismatch, which significantly restricts the conversion efficiency of the c-Si solar cell to 19%. The efficiency is significantly lower than the theoretical value of 31.0% reported by Shockley.[5] Extensive studies have been performed to decrease the energy loss caused by spectral mismatch and to increase the device efficiency.[6–10]

[a]School of Chemical Engineering and Pharmaceutics, Henan University of Science and Technology, Luoyang, 471003, P. R. China. E-mail: blpan@haust.edu.cn
[b]School of Physics and Engineering, Henan University of Science and Technology, Luoyang, 471003, P. R. China
[c]School of Physics and Optoelectronic Engineering, Guangdong University of Technology, Guangzhou 510006, P. R. China
[d]Department of Chemistry and Chemical Engineering, Ankang University, Ankang 725000, P. R. China

However, most methods have disadvantages of high costs and complex preparation processes, which limit their applications in solar cells. Quantum cutting (QC) is a promising method to increase the efficiencies of solar cells. According to the design of a luminescent layer on top of the solar cell, one incident UV-Vis photon was converted to two NIR photons, efficiently absorbed by the c-Si solar cell. Therefore, the energy loss caused by thermalization could be effectively suppressed and thus the efficiency of the solar cell could be increased.[11,12]

Rare-earth (RE) ions are optimal candidates for QC owing to their abundant energy levels. Considering the energy levels of lanthanides, the Yb^{3+} ion has a single excited state at approximately 10 000 cm^{-1} and exclusively emits NIR photons at ~1000 nm, which correspond to the strongest spectral response of c-Si. Therefore, many studies have been focused on the RE–Yb^{3+} co-doped system (RE = Eu^{2+},[13,14] Ce^{3+},[15–17] Pr^{3+},[18–20] Er^{3+},[21,22] and Tb^{3+} (ref. 23 and 24)) in recent years. The RE ion absorbs one incident UV-Vis photon and transfer its energy to two Yb^{3+} ions by cooperative energy transfer (CET) with an optimal QE of approximately 200%.[25,26] However, the NIR luminescent intensity of the Yb^{3+} ion is significantly lower than that of its counterpart in the UV-Vis region. In addition, charge transfer state (CTS) could emerge for Yb^{2+}–O^{2-} or Yb^{3+}–O^{2-}.[13,16] These disadvantages have decreased the practical QE for the RE–Yb^{3+} couple and further limited its application to solar cells.

Nd^{3+} is an another RE ion with NIR luminescence in the range of 800–1500 nm. The Nd^{3+} fluorescence intensity at NIR wavelengths is higher than that of Yb^{3+}; in addition, no CTS emerges during the ET process. The NIR luminescence of Nd^{3+} is in the wavelength range of 800–1500 nm, significantly broader than that of Yb^{3+} of 900–1100 nm; and the spectral response range to c-Si could be broadened. Therefore, the RE–

Nd^{3+} couples have larger potentials to increase the efficiency of c-Si. However, only a limited number of studies analyzed the RE–Nd^{3+} co-doped system and its QC property.[27,28] The Eu^{2+} ion is a typical broadband sensitizer owing to the allowed 4f → 5d transition; its fluorescence spectra have been controlled by the crystal field of the matrix. The emission spectrum of the Eu^{2+} ion in a $SrAl_2O_4$ matrix well overlaps with the Nd^{3+} excitation spectrum. The energy of the Eu^{2+}:$4f^7 \rightarrow 4f^65d^1$ transition is twice that of the Nd^{3+}:${}^4F_{3/2} \rightarrow {}^4I_{11/4}$ transition, which enables a DC process between Eu^{2+} and Nd^{3+}.

In this study, we report an efficient QC process in Eu^{2+}–Nd^{3+}-co-doped $SrAl_2O_4$ microcrystals. The fluorescence spectra of Eu^{2+} and Nd^{3+} were recorded to verify the ET process. The dependence of the visible and NIR emission intensities on the Nd^{3+} concentration was studied to investigate the ET mechanism. The decay lifetime of Eu^{2+}, ET rate, and QE were also evaluated. The aim of this study was to utilize the broadband UV-Vis part of the solar spectrum to enhance the NIR responses of c-Si solar cells.

2. Experimental

Microcrystals of $SrAl_2O_4$:$0.01Eu^{2+}$,xNd^{3+}(x = 0, 0.01, 0.02, 0.05, 0.10, 0.15 in mol) were synthesized by a conventional solid-state reaction method, using $SrCO_3$ (99.5%), Al_2O_3 (99.5%), Eu_2O_3 (99.9%), Nd_2O_3 (99.9%), and H_3BO_3 (99.5%) as raw materials. All of the raw materials were dried at 100–150 °C for 10–12 h in the drying oven to remove the residual water. The starting materials were weighed by the designed stoichiometric proportion, a 5 mol% excess of H_3BO_3 was added as a flux, and then wet-mixed with the absolute alcohol (>97%) for 2–3 h in the agate mortar. After mixing, the powder was dried in the oven for 12 h at 100 °C. The powder was sintered in a corundum crucible under reducing atmosphere, which was supplied by the mixed gas of 95% argon and 5% hydrogen. Reactions were performed in a vertical high-temperature tube furnace at 1200 °C for 3–5 h, and then cooled to room temperature. Both of the heating and annealing rates are 3 °C min^{-1}.

In order to identify the phase structures of the as-synthesized samples, powder X-ray diffraction (XRD) measurements were performed using a Rigaku D/max-2000 powder diffractometer with Cu K_α radiation (1.5405 Å) in the range of 20–70°. The optical properties were measured using an Edinburgh Instruments FLS920 spectrofluorometer; excitation and emission spectra, decay curves, and lifetimes of the products were obtained. All of the measurements were performed at room temperature.

3. Results and discussion

3.1 Structure behavior

Fig. 1 shows XRD patterns of the products. Compared with the standard data (JCPDS card no. 34-0379), all of the diffraction peaks corresponded to a pure monoclinic α-$SrAl_2O_4$ phase with lattice parameters of a = 5.069(2) Å, b = 8.799(7) Å, and c = 9.759(9) Å. In addition, no allotropic or impurity phases appeared in the patterns, which implies that the pure α-$SrAl_2O_4$ crystalline phase was obtained and that the Eu^{2+} and Nd^{3+} ions were thoroughly incorporated into the matrix. Fig. 1 also shows that the diffraction peaks shifted to higher angles 2θ with the increase in the Nd^{3+} concentration. The reason is that Eu^{2+} (112 pm) and Nd^{3+} (99.5 pm) ions substituted Sr^{2+} (113 nm) ions in α-$SrAl_2O_4$, and the radii of the RE ions are smaller than that of Sr^{2+}. According to the Scherrer's equation $n\lambda = 2d \sin\theta$, therewith, the interplanar spacing decreased.

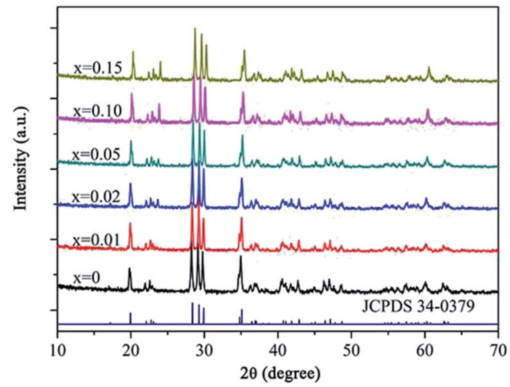

Fig. 1 The XRD patterns of Eu^{2+} single doped and Eu^{2+},Nd^{3+} codoped $SrAl_2O_4$.

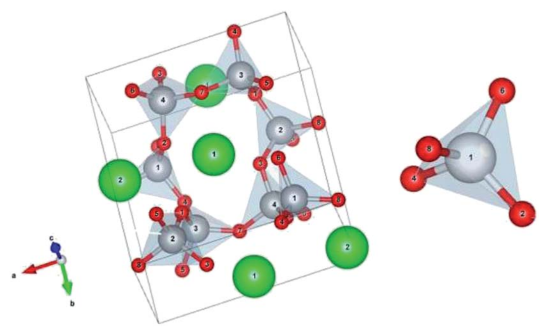

Fig. 2 Crystalline structure of α-$SrAl_2O_4$.

In order to further interpreted the substitution of Sr^{2+} by RE ions, Fig. 2 shows the crystalline structure of the monoclinic α-$SrAl_2O_4$. In the crystal lattice of α-$SrAl_2O_4$, each aluminium (Al) atom is surrounded by four oxygen (O) atoms, forming AlO_4 tetrahedra. Furthermore, the AlO_4 tetrahedra combine with each other by Al–O bonds to form a six-membered ring with a cavity volume of approximately 398 × 10^6 pm^3; the Sr^{2+} ions are located at the centers of the rings. The hexagon rings supply a sufficient space to facilitate the substitution of Sr^{2+} ions by RE ions.

3.2 ET between Eu^{2+} and Nd^{3+}

Fig. 3 gives the fluorescent spectra of the $SrAl_2O_4$:$0.01Eu^{2+}$ and $SrAl_2O_4$:$0.01Nd^{3+}$ samples. Fig. 3(a) and (b) show that both the excitation and emission spectra of Eu^{2+} ion exhibit typical broadband characteristic in $SrAl_2O_4$ matrix, covering the UV range of 250–400 nm and visible range of 450–600 nm, respectively. In the $SrAl_2O_4$:$0.01Nd^{3+}$ sample, the excitation spectrum was obtained by monitoring the 1064 nm emission, which is in

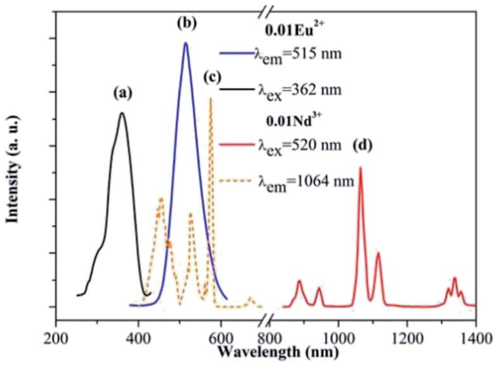

Fig. 3 The fluorescence spectra of $SrAl_2O_4$:0.01$Eu^{2+}$and $SrAl_2O_4$:0.01Nd^{3+} samples. (a) The excitation spectrum of Eu^{2+} (λ_{em} = 515 nm) in the $SrAl_2O_4$:0.01Eu^{2+} sample, (b) the emission spectrum of Eu^{2+} (λ_{ex} = 362 nm) in the $SrAl_2O_4$:0.01Eu^{2+} sample, (c) the excitation spectrum of Nd^{3+} (λ_{em} = 1064 nm) in the $SrAl_2O_4$:0.01Nd^{3+} sample, (d) the emission spectrum of Nd^{3+} (λ_{ex} = 520 nm) in the $SrAl_2O_4$:0.01Nd^{3+} sample.

the range of 400–700 nm. It was noticed that the excitation peak of Nd^{3+} at 520 nm was overlapped well with the emission spectrum of Eu^{2+} ion, implying the possible ET form Eu^{2+} to Nd^{3+} in $SrAl_2O_4$ matrix. Moreover, under the 520 nm excitation, the representative emission spectrum of Nd^{3+} emerges in the NIR range of 800–1200 nm correspondence with the strongest absorption of c-Si solar cells.

In order to confirm the ET process between Eu^{2+} and Nd^{3+}, the dependence of the emission intensities in both visible and NIR regions on the doping concentration of Nd^{3+} is shown in Fig. 4. All of the emission spectra were recorded under the 362 nm excitation (Eu^{2+}:$4f^65d^1 \rightarrow 4f^7$ allowed transition). In the visible region, the emission intensities of Eu^{2+} monotonously decreased with the increase in the Nd^{3+} concentration. Since the concentration of Eu^{2+} was fixed to be 0.01 mol in every sample, the decreasing of emission intensity was ascribed to the ET from Eu^{2+} to Nd^{3+}. On the contrary, the NIR emission intensities of Nd^{3+} rapidly increased with the Nd^{3+} concentration in the range of 0.01 to 0.10 owing to the ET from Eu^{2+} to Nd^{3+}. With the further increase in the Nd^{3+} concentration, at 0.15, the emission intensity of Nd^{3+} was significantly lower than that of the 0.10

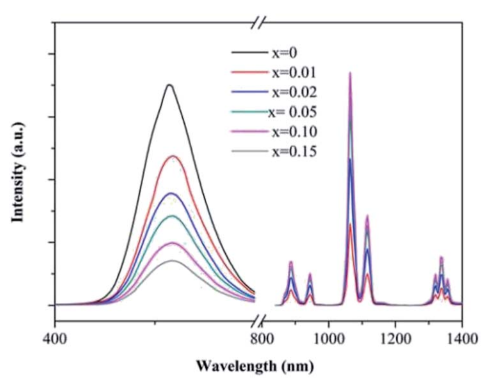

Fig. 4 Concentration-dependent emission spectra of $SrAl_2O_4$:0.01Eu^{2+}, xNd^{3+} (x = 0–0.15) under 362 nm excitation.

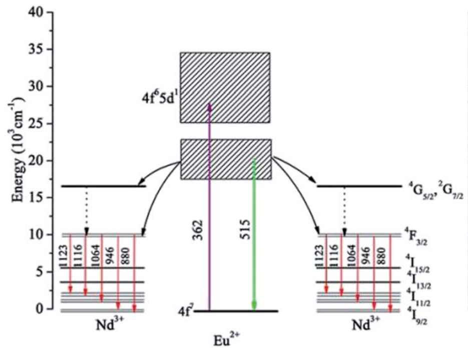

Fig. 5 Schematic energy level diagrams of Eu^{2+}, Nd^{3+}, showing the QC process between Eu^{2+} and Nd^{3+} under 362 nm excitation.

sample, which indicates that concentration quenching (CQ) occurred among the Nd^{3+} ions.

3.3 ET mechanism

In order to illustrate the ET mechanism in detail, schematic energy diagrams of Eu^{2+} and Nd^{3+} are presented in Fig. 5. As the excitation state of Eu^{2+}:$4f^65d^1$ was split to two energy levels in the $SrAl_2O_4$ matrix, the ET process from Eu^{2+} to Nd^{3+} can be described as follow. Under the 362 nm excitation, the Eu^{2+}:$4f^7 \rightarrow 4f^65d^1$ transition occurred and the photons populated the higher $4f^65d^1$ level, which then relaxed to the lower $4f^65d^1$ state by Stokes shift. Majority of the photons, which occupied the Eu^{2+}:$4f^65d^1$ (lower) state, transferred their energies to the Nd^{3+}:$^4F_{3/2}$ state. The energy gap of the Eu^{2+}:$4f^65d^1 \rightarrow 4f^7$ transition is approximately twice that of the Nd^{3+}:$^4F_{3/2} \rightarrow {}^4I_{11/2}$ transition; therefore, this ET process is proposed as a DC process with a CET mechanism. In addition, transition of Nd^{3+}:$^4F_{3/2} \rightarrow {}^4I_{9/2}$ also occurred due to the sensitization of Eu^{2+}, during this process, Eu^{2+} ion absorbed on incident visible photon and transferred its energy to Nd^{3+}, emitted one NIR photon. Therefore, the 880 nm and 946 nm NIR emission intensities of Nd^{3+} were enhanced.

Fig. 6 displays the spectral response of Nd^{3+} ion to solar spectrum and silicon absorption. It can be seen that the emission spectrum of Nd^{3+} lies in the range of 800–1200 nm, which is much broader than that of Yb^{3+} and meets the strongest spectral response of c-Si solar cells. Moreover, the NIR emission of Nd^{3+} has been enhanced by the CET process, and then efficiently utilized by the c-Si solar cell. In addition, the excitation spectrum of Nd^{3+} in the range of 400–700 nm is a typical broadband, enabling absorption of the strongest emission of the solar spectrum. In a word, the $SrAl_2O_4$:Eu^{2+},Nd^{3+} phosphor can convert the UV-Vis broadband of the solar spectrum to the NIR range, which could be potentially employed to increase the conversion efficiency of c-Si solar cells by reducing the thermalization loss.

3.4 Decay curves and ET efficiency

The decay curves for the Eu^{2+}:$4f^7 \rightarrow 4f^65d^1$ transition at 515 nm are plotted for different Nd^{3+} concentrations in Fig. 7. The

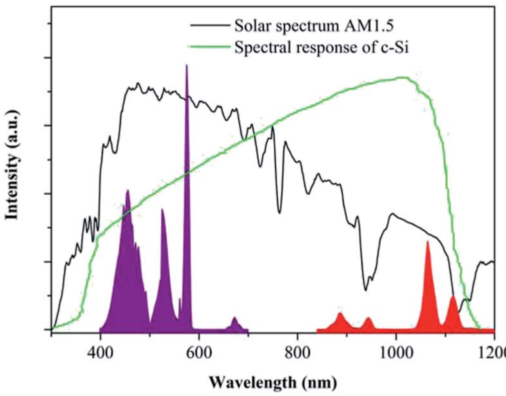

Fig. 6 The excitation and emission spectra of $SrAl_2O_4$:Eu^{2+},Nd^{3+}, indicating the spectral match and spectral response of Eu^{2+} and Nd^{3+}. The AM 1.5 G solar spectrum and spectral response of c-Si in this spectral region are shown in the background as references.

experimental lifetime (τ_m) of the Eu^{2+} 515 nm emission can be calculated by:

$$\tau_m = \frac{1}{I_0}\int_0^{\infty} I(t)\mathrm{d}t \quad (1)$$

where I_0 is the luminescence intensity at $t = 0$, while $I(t)$ is the luminescence intensity at t after the excitation source was cut-off. The Eu^{2+} single doped sample exhibited an approximately single-exponential decay curve with a lifetime τ_m of 6.1 μs. With the increase in the Nd^{3+} concentration from 0 to 0.10 mol, the decay curves gradually deviated from single-exponential curves, and the lifetime τ_m decreased to 4.9, 3.8, 2.1, and 1.4 μs gradually. As the Eu^{2+} concentration is set to 0.01 mol in all of the samples, the decreasing lifetime and non-single exponential decay curves were attributed to the introduction of extra decay pathways, such as the CET from Eu^{2+} to Nd^{3+}.

In order to further illuminate the ET process between Eu^{2+} and Nd^{3+}, the energy transfer (ET) rate dependence on the Nd^{3+} concentration has been investigated. Since the lifetime of Eu^{2+} (donor) decreases with the increasing in the Nd^{3+} (acceptor) concentration, the CET from Eu^{2+} to Nd^{3+} is primarily a non-radiative process,[29] which can be modeled by the Forster–Dexter theory of non-radiative ET processes.[30] Furthermore, the dipole–dipole interaction is essential for this CET process according to previous reports.[31,32]

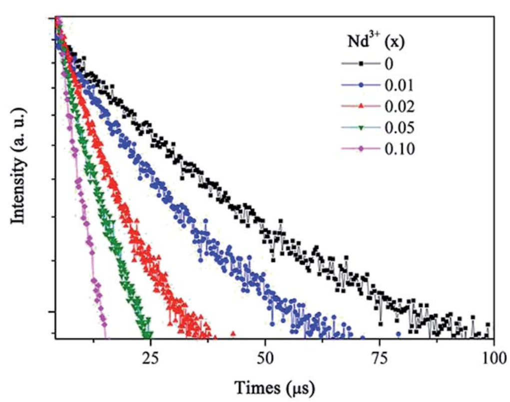

Fig. 7 Decay lifetimes of the Eu^{2+}:$4f^65d^1 \rightarrow 4f^7$ emission (515 nm) under 362 nm excitation.

Table 1 The energy transfer efficiency (P_{DA}) and energy transfer efficiency (η_{DA}) with different Nd^{3+} concentration in Eu^{2+}–Nd^{3+} codoped $SrAl_2O_4$ samples

Nd^{3+} (mol%)	P_{DA} (μs^{-1})	η_{DA} (%)
0.01	0.041	19.7
0.02	0.099	37.7
0.05	0.312	65.6
0.10	0.550	77.1

The macroscopic ET rate P_{DA} of the dipole–dipole interaction can be estimated by the lifetime of the donor ions (Eu^{2+}) using:[33]

$$P_{DA} = \frac{1}{\tau} - \frac{1}{\tau_0} \quad (2)$$

where τ_0 and τ denote the lifetimes of the donor emissions in the Eu^{2+} single-doped and Eu^{2+}–Nd^{3+} co-doped samples, respectively.

Using eqn (2), the ET rates of the Eu^{2+}–Nd^{3+} co-doped samples can be evaluated.

As the non-radiative transition in the donors can be neglected according to Dexter,[30] the ET efficiency (η_{DA}) between Eu^{2+} and Nd^{3+} can be calculated by:[34]

$$\eta_{DA} = \frac{P_{DA}\tau_0}{1 + P_{DA}\tau_0} \quad (3)$$

P_{DA} and η_{DA} are calculated as a function of the Nd^{3+} concentration and listed in Table 1. The ET rate and efficiency significantly increased upon the Nd^{3+} introduction. For the $SrAl_2O_4$:0.01Eu^{2+},0.01Nd^{3+} sample, P_{DA} and η_{DA} are 0.041 μs^{-1} and 19.7%, respectively. With the increase in the Nd^{3+} concentration to 0.10 mol%, η_{DA} increases to approximately 77.1% with $P_{DA} = 0.55\ \mu s^{-1}$. The increasing of P_{DA} and η_{DA} with the introduction of Nd^{3+} verified that the ET occurred from Eu^{2+} to Nd^{3+}.

In addition, the theoretical QE of the Eu^{2+}–Nd^{3+} pair was evaluated by:[35]

$$QE = \eta_{Eu}(1 - \eta_{DA}) + 2\eta_{DA} \quad (4)$$

where η_{Eu} is the QE of Eu^{2+}, which is supposed to be 1 according to ref. 14. The estimated theoretical QE are 119.7%, 137.7%, 165.6%, and 177.1% for the $x = 0.01$, 0.02, 0.05, and 0.10 Nd^{3+} doped samples, respectively. It is worth noting that the actual QE was lower than the theoretical value owing to the Eu^{2+} non-radiative transition.

4. Conclusions

A broadband NIR QC was achieved in the $SrAl_2O_4$:Eu^{2+},Nd^{3+} phosphors. Under the 362 nm excitation, the Nd^{3+} ion emitted two NIR photons in the range of 800–1200 nm by the CET process from the Eu^{2+}:$5d^1$ state to the Nd^{3+}:${}^4F_{3/2}$ state. The optimal QE was 177.1% before the QC occurred. This material can efficiently utilize the broadband solar spectrum in the UV-Vis region; therefore, it might reduce the thermalization loss and thus has significant potentials to increase the conversion efficiency of c-Si solar cells.

Conflicts of interest

There are no conflicts to declare.

Acknowledgements

This work was supported by the National Natural Science Foundation of China (No. 61775052 and 51675162), Education Department Project of Henan Province (No. 18B150005), Open Research Fund of State Key Laboratory of Transient Optics and Photonics, Chinese Academy of Sciences (SKLST201203), Foundation for University Key Teacher of Henan Province (No. 2013071), Natural Science Fund of Education Department of Shaanxi Provincial Government (Grant No. 16JK1018), Natural Science Fund and Subject Merging Fund of Ankang University for high-level talents (Grant No. 2016AYQDZR05 and 2017AYJC01), and Key Project of Industrial Science and Technology of Shaanxi Province (No. 2016GY-196).

Notes and references

1 M. Gratzel, *Nature*, 2001, **414**, 338–344.
2 A. Goetzberger, C. Hebling and H. W. Schock, *Mater. Sci. Eng., R*, 2003, **40**, 1–46.
3 N. N. Zhang, Y. Zhang, J. Bao, F. Zhang, S. Yan, S. Sun and C. Gao, *Chin. Opt. Lett.*, 2017, **15**, 063501.
4 S. Gu, P. Zhu, R. Lin, M. Tang, S. Zhu and J. Zhu, *Chin. Opt. Lett.*, 2017, **15**, 093501.
5 W. Shockley, *J. Appl. Phys.*, 1961, **32**, 1402–1403.
6 I. M. Dharmadasa, *Sol. Energy Mater. Sol. Cells*, 2005, **85**, 293–300.
7 A. J. Nozik, *Chem. Phys. Lett.*, 2008, **457**, 3–11.
8 D. Timmerman, I. Izeddin, P. Stallinga, I. N. Yassievich and T. Gregorkiewicz, *Nat. Photonics*, 2008, **2**, 105–109.
9 B. S. Richard and A. Shalav, *Synth. Met.*, 2005, **154**, 61–64.
10 B. M. Van Der Ende, L. Aarts and A. Meijerink, *Phys. Chem. Chem. Phys.*, 2009, **11**, 11081–11095.
11 T. Trupke, M. A. Green and P. Würfel, *J. Appl. Phys.*, 2002, **92**, 1668–1674.
12 B. S. Richards, *Sol. Energy Mater. Sol. Cells*, 2006, **90**, 1189–1207.
13 J. J. Zhou, Y. X. Zhuang, S. Ye, Y. Teng, B. Zhu, J. H. Xie and J. R. Qiu, *Appl. Phys. Lett.*, 2009, **95**, 141101.
14 H. Lin, D. Q. Chen, Y. L. Yu, Z. F. Shan, P. Huang, A. P. Yang and Y. S. Wang, *J. Alloys Compd.*, 2011, **509**, 3363–3366.
15 X. Liu, Y. Teng, Y. Zhuang, J. Xie, Y. Qiao, G. Dong, D. Chen and J. Qiu, *Opt. Lett.*, 2009, **34**, 3565–3567.
16 H. Lin, S. Zhou, H. Teng, Y. Li, W. Li, X. Hou and T. Jia, *J. Appl. Phys.*, 2010, **107**, 043107.
17 Y. Tai, X. Li, X. Du, B. Pan and G. Yuan, *RSC Adv.*, 2018, **8**, 23268–23273.
18 A. Jaffrès, B. Viana and E. van der Kolk, *Chem. Phys. Lett.*, 2012, **527**, 42–46.
19 C. Ming, F. Song, L. An and X. Ren, *Curr. Appl. Phys.*, 2014, **14**, 1028–1030.
20 Y. Tai, X. Du, X. Li, B. Pan, G. Yuan and H. Wang, *J. Photochem. Photobiol., A*, 2018, **360**, 64–70.
21 J. J. Eilers, D. Biner, J. T. van Wijngaarden, K. Krämer, H.-U. Güdel and A. Meijerink, *Appl. Phys. Lett.*, 2010, **96**, 151106.
22 L. Aarts, B. M. van der Ende and A. Meijerink, *J. Appl. Phys.*, 2009, **106**, 023522.
23 S. Ye, B. Zhu, J. Chen and J. Luo, *Appl. Phys. Lett.*, 2008, **92**, 141112.
24 X. Liu, S. Ye, Y. Qiao, G. Dong, B. Zhu, D. Chen, G. Lakshminarayana and J. Qiu, *Appl. Phys. B*, 2009, **96**, 51–55.
25 Q. Zhang, C. Yang, Z. Jiang and X. Ji, *Appl. Phys. Lett.*, 2007, **90**, 061914.
26 Q. Zhang, G. Yang and Z. Jiang, *Appl. Phys. Lett.*, 2007, **91**, 051903.
27 H. hang, Y. Wang and L. Han, *J. Appl. Phys.*, 2011, **109**, 053109.
28 Y. Tai, G. Zheng, H. Wang and J. Bai, *J. Photochem. Photobiol., A*, 2015, **303–304**, 80–85.
29 L. G. Van Uiter and L. F. Johnson, *J. Chem. Phys.*, 2004, **44**, 3514.
30 D. L. Dexter, *J. Chem. Phys.*, 1953, **21**, 836–850.
31 M. A. Chamarro and R. Cases, *J. Non-Cryst. Solids*, 1989, **107**, 178–186.
32 S. Tanabe, T. Kouda and T. Hanada, *Opt. Mater.*, 1999, **12**, 35–40.
33 Z. Nie, J. Zhang, X. Zhang, S. Lü, X. Ren, G. Zhang and X. Wang, *J. Solid State Chem.*, 2007, **180**, 2933–2941.
34 R. Reisfeld and N. Lieblich-Soffer, *J. Solid State Chem.*, 1979, **28**, 391–395.
35 D. Chen, Y. Yu, H. Lin, P. Huang, Z. Shan and Y. Wang, *Opt. Lett.*, 2010, **35**, 220–222.

